JOINT INSTITUTE FOR NUCLEAR RESEARCH
Flerov Laboratory of Nuclear Reactions

FINAL REPORT ON THE
SUMMER STUDENT PROGRAM

Experimental study of evaporation residue cross-sections in a complete fusion reactions leading to Hg.

Supervisor:
Viacheslav Yurievich Vedeneev

Student:
Maxim Vitalievich Romanovskiy, Russia, Tomsk Polytechnic University

Participation period:
June 30 – August 10

Dubna, 2019

ABSTRACT

The fusion excitation functions of *xn*-evaporation channels in the reactions leading to *Hg* isotopes were studied by using the well-known catcher foil method. The beam of ^{36}Ar was used to produce *Hg* isotopes in the fusion reaction $^{36}Ar(^{148}Sm,xn)^{184-x}Hg$. An improved version of the catcher foil method used in this experiment is described. The data processing required for this method is also outlined.

The cross-sections of evaporation residua in a full fusion reaction $^{36}Ar+^{148}Sm$ had been calculated and results are discussed. This reaction is of great interest, because of non-sphericity of reacting nuclei in comparison to spherical nuclei reaction $^{40}Ar(^{144}Sm, xn)^{184-x}Hg$.

The new results will make it possible to refine theoretical models of fusion that can be used in the study of superheavy nuclei.

INTRODUCTION AND MOTIVATION OF THE EXPERIMENT

In experiments aimed at studying the chemical properties of superheavy elements, it was found that the 112th element (*Cn*) has an increased volatility compared to mercury, nevertheless is its chemical analogue [1]. That is why *Hg* was chosen for the experiment.

The motivation for performing these experiments is the study of fusion reactions with target nuclei near the 82-neutron closed shell. A systematic study of evaporation residue cross-sections over excitation energies close to the Coulomb barrier was carried out using the nuclear reaction $^{36}Ar + ^{148}Sm$ producing the isotopes of mercury.

Another motivation of performed experiment was the calculation of separation efficiency for mercury-like nuclei at MASHA (Mass Analyzer of Super-Heavy Atoms) facility. A well-known ISOL (Isotope Separation On-Line) methodic [2] implemented at the MASHA facility is widely used in nuclear reactions physics and a test complete fusion reactions $^{40}Ar + ^{144}Sm$ and $^{40}Ar + ^{166}Er$ were performed with a synthesis of short-lived *Hg* and *Rn* isotopes after neutron evaporation. This methodic could provide a secondary beam of radioactive nuclei of low energy that could be analyzed in a

magneto-optical layout. By comparison, of gained yields and cross-sections with another experiment to be held it could be possible to calculate total separation efficiency of the installation, depending on materials used in thermalization block unit. The data for the fusion cross-sections of reactions, listed above, is absent in a literature.

The stabilizing effect of shells is reflected in the distribution of the isotope yields of the evaporation residues. The yields in this study were determined by using the catcher foil method.

EXPERIMENTAL SETUP

The catcher foil method [3] was used for this experiment. In this method a thin aluminum foil is placed near to and downstream of the target. This foil, also referred to as the catcher, was used to stop the reaction products in the first phase of the experiment. Then, in the second phase, the foil shifted to a position in front of the detector, which measures the alpha particles of decay products and their daughter nuclei. In our case, an improved version of this method was used by replacing the traditional single foil with a five-foil setup. This increases the energy resolution from ~250 keV to ~80 keV. The foils used in this experiment were made of aluminum, and their effective thickness was adjusted to stop all of the reaction products and, at the same time, to concentrate the distribution of products primarily on the center foil. A special apparatus was made specifically for this experiment containing 5 silicon detectors placed adjacent to each other, and 5 aluminum foils placed on a specialized retraction system (*Figure 1*).
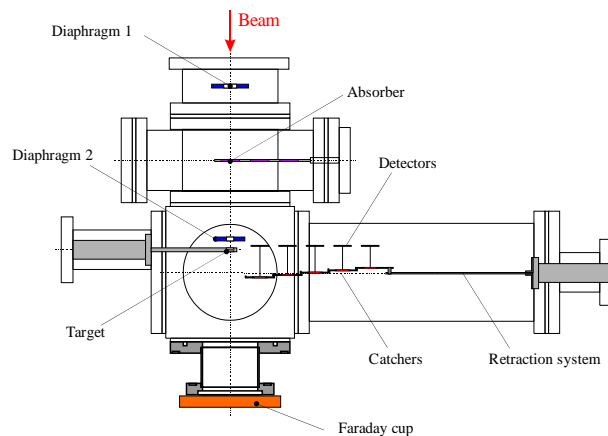

Figure 1. *Schematics of measurement setup.*

The experiment was carried out at cyclotron U400M in FLNR at the JINR laboratory. The energy step of the heavy ion beams was ≈ 3 MeV. The beam energy was adjusted by using one from four nickel absorption foils with different thicknesses. Nickel foils with thicknesses of 2.7, 4.95, 10.3 and 16.9 μm were placed on a rotating construction. The accuracy of linear motion was 0.1 mm and the rotational accuracy was 0.5°. After passing through the absorbing foils a beam having the required energy then hit the target. A ^{148}Sm target of average density ≈ 315 μg/cm^2, and an ^{36}Ar beam were used. The reaction products were caught by a system of five aluminum foils located 18.2 mm behind the target. The foils had a circular shape with a diameter of 20 mm and a thickness of 0.75 μm. A schematic of the retraction system is shown on a *Figure 2*.
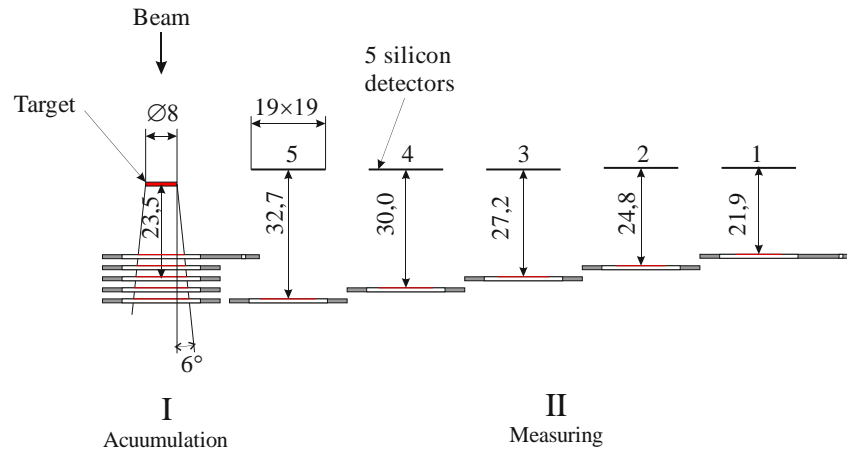

Figure 2. *Schematics of the retraction system. The system consists of 5 stopping Al foils (catchers) and 5 Si detectors.*

This system was operated by a linear and rotary mechanical feedthrough. During the experiment the system of *Al* foils was in one of two arrangements. Firstly, the foils were arranged in a succession behind the target to stop decay products, and the accumulation took t_b seconds (while the beam was on the target). In the second arrangement the foils were moved to a side-by-side arrangement in front of the silicon detectors, which measured alpha particles of decay products exposed on the foils for time t_d (while the beam was off). Due to the use of beam interruption and the linear displacement of the foils, we are able to identify products by their half-life with a

resolution of ~0.1 s. Times t_b and t_d were chosen based on the half-lives of the reaction products, and was typically set to 10 seconds.

The shifting of the foil positions repeated periodically during the entire measurement. The transitions were synchronized with the interruption of the ion beam and data acquisition system. A "CompactRIO" controller from "National Instruments" controlled the entire system.

DETECTION OF REACTION PRODUCTS

During the period of irradiation more or less nuclei estimate undecayed in foils. The difference from one isotope to another is only how fast the number of nuclei coming to beam time becomes equilibrium. This number should be established as N_0. That was firstly. Secondly, the transition time between two states "on beam" and "on measurement" is small, but finite and defined. By looking on a time/energy graph it was defined as ~0.3 s. Defined it as t_m. Also, suggest t_b and t_d as times on beam and detection time, respectively. So, all the period of irradiation-measurement will consists of $t_b + 2t_m + t_d$ and equals 20 seconds.
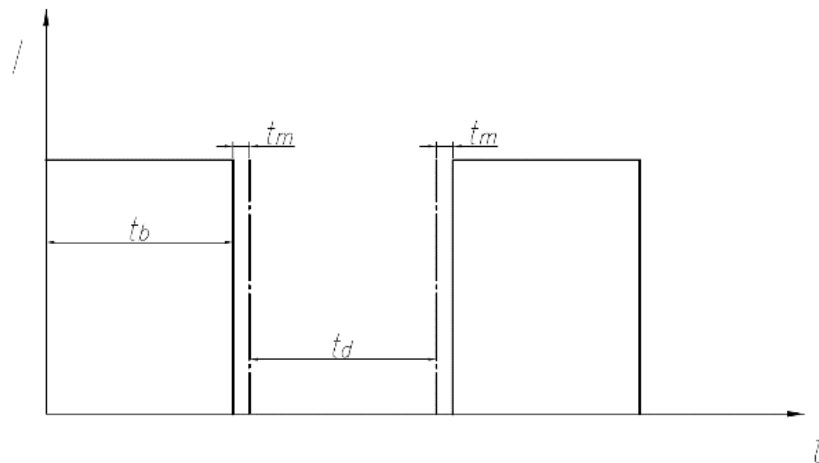

Figure 3. *Time graph for irradiation and detection.*

On a *Figure 3*, the time graph of irradiation is presented. This is a simplified model where *I* is always constant and represents average current within all cycles during run. During irradiation period t_b the number of estimated nuclei from N_0 is

$$N = N_0 e^{-\lambda t_b}; \tag{1}$$

A yield of newborn nuclei during this period is N_b

$$N_b = \frac{\beta\sigma}{\lambda}\left(1 - e^{-\lambda t_b}\right); \tag{2}$$

where β is characteristics of target and beam and σ is its cross-section.

$N+N_b$ nuclei goes to detection time and after the period of $2t_m+t_d$ again comes to the beam as a stationary regime with N_0 nuclei.

$$(N + N_b)e^{-\lambda(2t_m+t_d)} = N_0; \tag{3}$$

$$\left(N_0 e^{-\lambda t_b} + N_b\right)e^{-\lambda(2t_m+t_d)} = N_0; \tag{4}$$

$$N_0 = \frac{N_b e^{-\lambda(2t_m+t_d)}}{1 - e^{-\lambda(2t_m+t_d+t_b)}}; \tag{5}$$

By the beginning of detection, the number of nuclei was N_d:

$$N_d = N_0 e^{\lambda(t_m+t_d)} = \frac{\beta\sigma}{\lambda}\left(1 - e^{-\lambda t_b}\right)\left(\frac{e^{-\lambda t_m}}{1 - e^{-\lambda(2t_m+t_b+t_d)}}\right); \tag{6}$$

For one cycle detector registered N_{det}^{α} of nuclei:

$$N_{det}^{\alpha} = gN_d\left(1 - e^{-\lambda t_d}\right) = \frac{g\beta\sigma}{\lambda}\frac{(1-e^{-\lambda t_b})e^{-\lambda t_m}(1-e^{-\lambda t_d})}{1 - e^{-\lambda(2t_m+t_b+t_d)}}; \tag{7}$$

where g is geometrical registration efficiency unique for each detector.

Calculated coefficients for geometric efficiency for all detectors as a space percentage of covering the solid angle between a single foil to detector are listed in *Table 1*.

Table 1. Geometric efficiency for each detector.

Detector	Geometric efficiency (%)
1	4,9
2	3,95
3	3,37
4	2,84
5	2,43

From this equation, the cross-section could be found as:

$$\sigma = \frac{N_{det}^{\alpha}\lambda\left(1 - e^{-\lambda(2t_m+t_b+t_d)}\right)}{g\beta\left(1-e^{-\lambda t_b}\right)e^{-\lambda t_m}\left(1-e^{-\lambda t_d}\right)}; \tag{8}$$

with the correction for lifetime already.

6

DATA PROCESSING

During the experiment, products of the reactions were caught by the five-layer *Al* foil system. Then five silicon detectors situated in front of the foils after moving them away from the target detected the alpha particles from reaction product. For every reaction, a number of measurements for different projectile energies were made with an energy step of approximately 3 MeV.

The data from an experiment were processed using an "OriginPro" software. Raw data from each run and each detector were filtered to avoid signal splashes while foils transitions and were saved in an ASCII code. Then, the histograms of alpha energies from each foil were batch processed for deleting the background. In total, it was 30 runs.

Before the experiment every run with the different energy was simulated in GEANT4 using a channel-coupling model to compare the simulated and experimental graphs. An example for the reaction $^{36}Ar+^{148}Sm$ at the projectile energy of about 180 MeV is shown on a *Figure 4*.

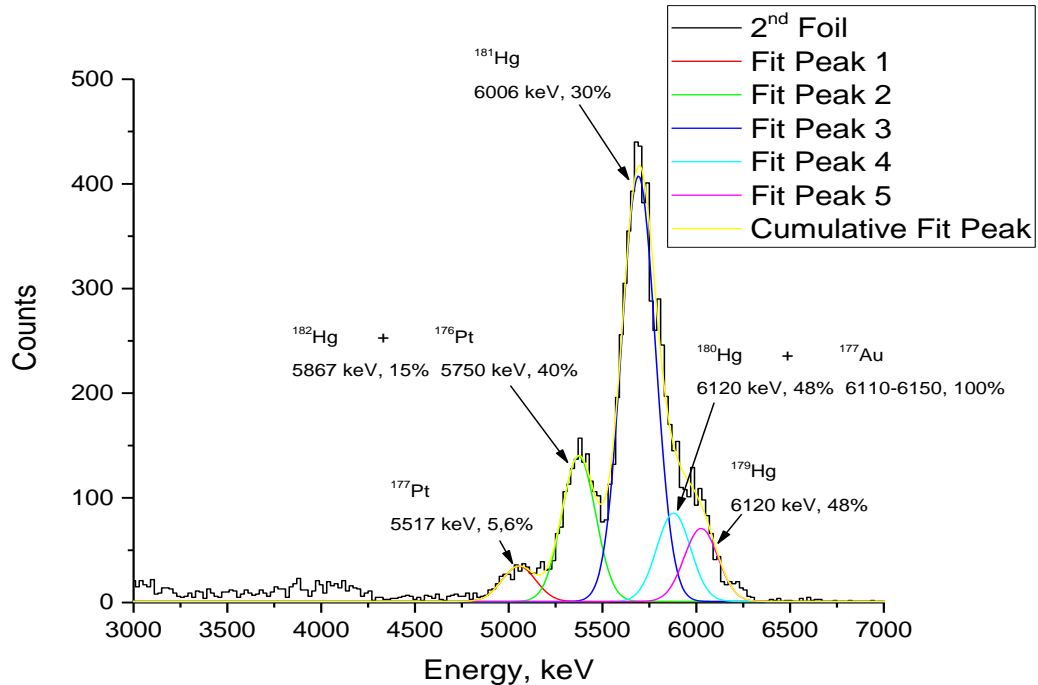***Figure 4.*** *An example of processed energy spectrum of the reaction $^{38}Ar + ^{184}Sm$ for energy 179,9 MeV with identified peaks. Single Gaussian fits are shown in colored lines.*

To identify the isotopes the Gaussian functions multiple peak fitting of histogram was used. The point of interest here are the mercury isotopes ^{180}Hg, ^{181}Hg and ^{182}Hg, which is *2n*, *3n*, *4n* evaporation channels, with alpha energies 6119 keV, 6006 keV and 5867 keV, respectively. The peak determination of these isotopes in a whole run is very complicated objective because of many unconcernities are inside. First of all, the resolution of detectors could differ from each other and from run to run due to its inner "dark" current's instability. Secondly, peaks could vary their energy positions, namely, "float" from one run to another due to the heating and thus, changing its dead layers. Thirdly, there is an unidentified quantity of isotopes could yield in a reaction (*xn-, ypxn-, yαxn-* evaporation channels, reactions of single- or multinucleon transfer et al.), because in that experiment a magnetic mass separation doesn't take part. Fourthly, during transitioning from the aluminum foil and the dead layers of detectors, alpha particles also lose some energies and a FWHM began to grow, which also hardens the peaks definition.

The isotopes were identified not only by its decay energy, but also by its lifetime. This shows how fast an isotopes decays within one measuring cycle. By choosing region and fitting the histogram it appears to be able to identify the isotope by its lifetime, as it is showed on a *Figure 5*.
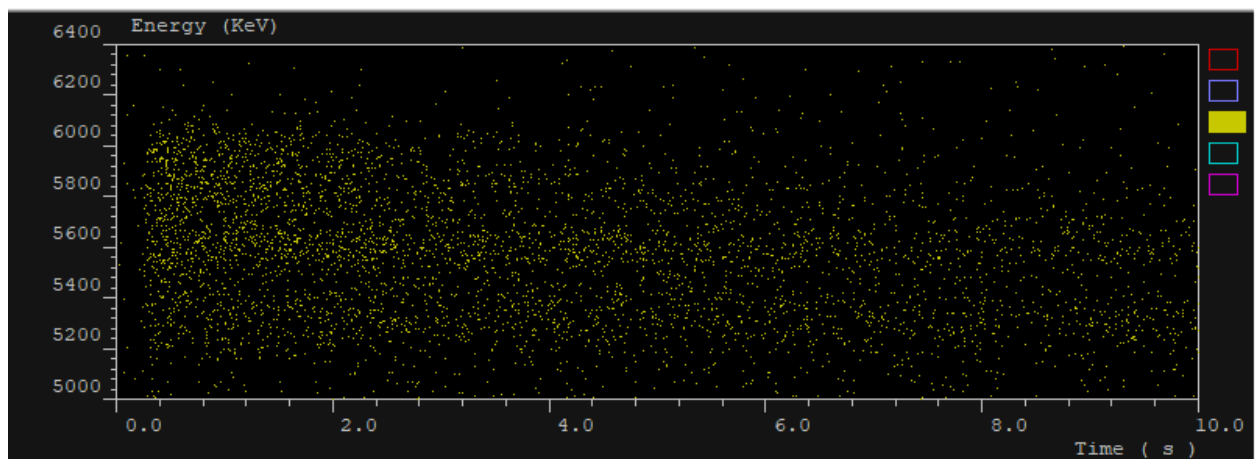

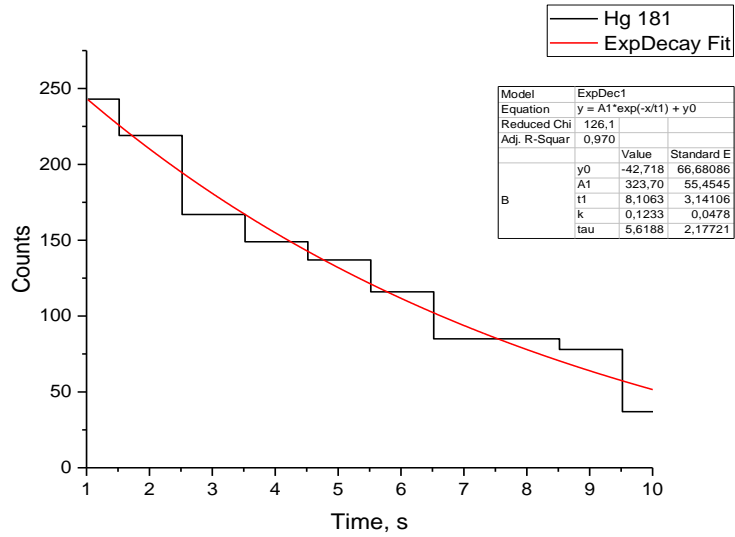**Figure 5.** *An example of time/energy graph from a single detector.*

Figure 6. *^{181}Hg decay histogram fitting.*

When the peaks were identified and fitted, the integration results were divided by 20, which is detector resolution and thus, a single bin width.

Integrals under the Gaussian curves corresponding to the alpha particles of reaction products were summed then for all detectors, taking into account their geometric efficiencies mentioned in *Table 2*.

The next stage was the corrections adjustment for the alpha-decay probability and the half-life for every isotope using the equations from above.

Cross sections of *2n*, *3n* and *4n* evaporation channels for each point of energy were calculated by using the formula

$$\sigma = \frac{(N \cdot M_{tg} \cdot Z \cdot e)}{(\rho \cdot N_A \cdot I)};$$
(9)

where N gives the obtained yields, M_{tg} is the mass number of the target, Z is the charge of the projectile, e is the elementary charge, ρ is the thickness (μg/cm^2), N_A is Avogadro's constant, and I is a beam current integral.

Cross section errors were calculated as the root of the quadratic sum of statistical error, error linked with data processing, error of the beam current measurement, and target measurement error.

Another used methodic for cross-section calculating is using a software written specially for this experiment inside FLNR using Visual C++. The example of it is

shown on *Figure 7*. This software could analyze raw data by applying deconvolution method to the chosen channels and calculate reaction cross-sections simultaneously. This could take into account not only *xn* channels, but *1pxn* and *1αxn* ones. The software could be used for scrupulous analysis of incoming data.
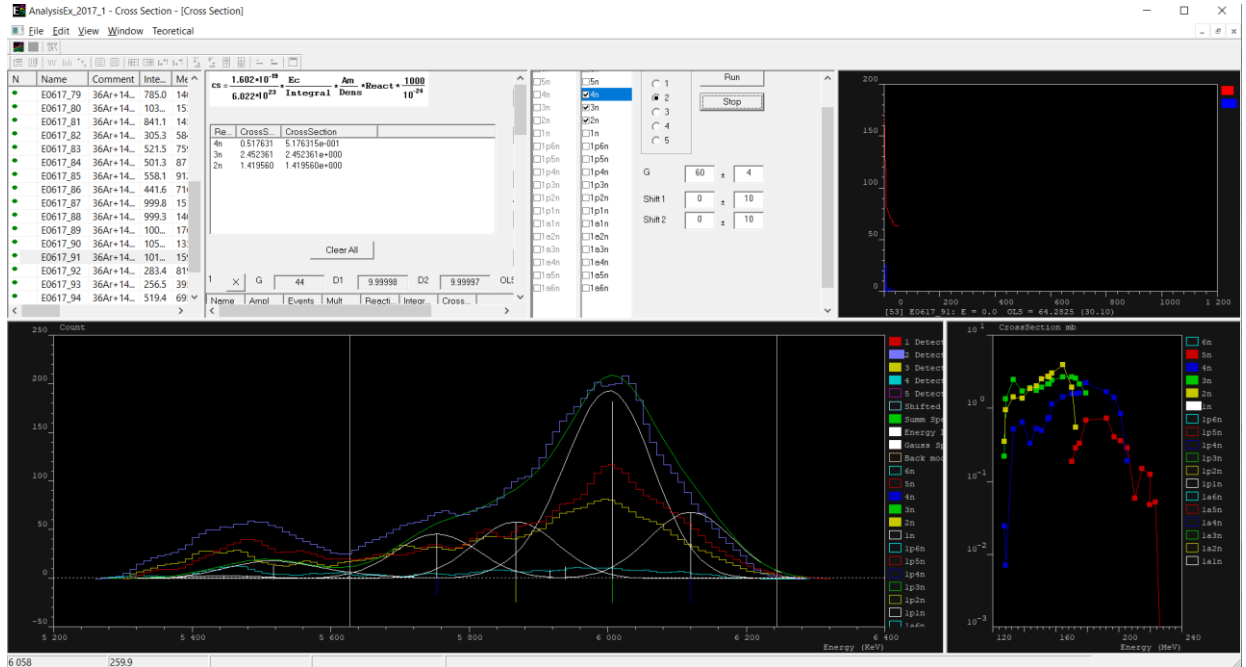

Figure 7. *An example window with data analysis. In the central window white lines marks the simulated data of defined σ for the chosen evaporation channels and its daughters over the gained data, which are marked with "ladder" histograms. Green line shows the sum spline.*

Beam energy was measured using a TOF method and high-speed digitizer, and energy losses were calculated using "SRIM" software [4], which includes nickel absorbers, titanium foil and losses inside the target material. For simplifying the losses inside thick target, a model of beam energy at the target middle was applied.

To measure the influence of energy dispersion as a function of beam energy separate measurements with decreasing beam energy were carried out. A ^{148}Sm target, 10,3μm thick, Ni foil and ^{36}Ar beam were used in this measurement. The beam energy was measured by using a semiconductor detector.

Table 2. Initial energies of the beams used in the listed reactions.

Reaction	Initial beam energy	Lowest final beam energy
$^{36}Ar + {}^{148}Sm$	~324 MeV	~144 MeV

Three measurements were performed, one without foil and two with different foil and target angles. Results are shown in *Figure 8*.
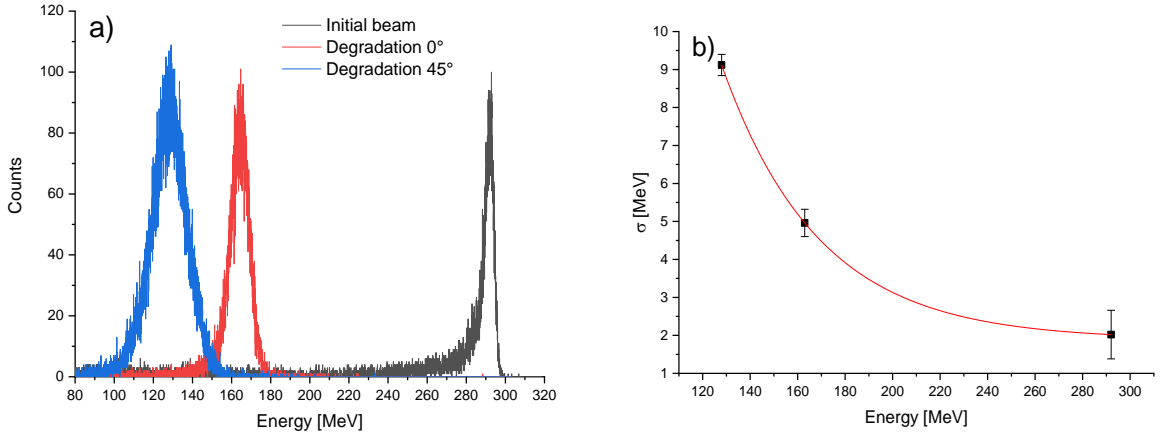

Figure 8. *a) Measured energy spectrum of the ^{36}Ar beam without target and Ni foil (blue) (FWHM = 4,76 MeV), with Ni foil having thickness 10,3 μm and angle 0°, target underlay with thickness 1,5 μm and target material Sm$_2$O$_3$ with thickness 0,48 μm (red) (FWHM = 11,69 MeV) and after rotating the foil by 45° (black) (FWHM = 21,49 MeV). b) The dependence of Gaussian sigma on beam energy in the middle of the target and exponential fit $\sigma = B \cdot e^{-E_c/t} + \sigma_0$ with parameters σ_0 = 1,89, B = 165,74 and t = 40,87. Energy measurement errors include detector resolution and accuracy of the Au foil angle measurement*

In the first measurement, having no foil or target, the measured beam energy distribution at FWHM was 4,7 MeV. By putting the foil and target into our system the FWHM of the energy distribution increased to 11,7 MeV. By rotating the foil by 45° the FWHM almost doubled to a value of 21,5 MeV, which is more than four times its initial value. To eliminate this undesirable effect, we decided to use the well-known mathematical Gold deconvolution method [5].

As a response function we used a Gaussian function of beam energy distribution dependent on the final beam energy

$$D = \frac{1}{w\sqrt{\frac{\pi}{2}}} \cdot e^{-2\left(\frac{E-E_c}{w}\right)^2};$$
(10)

This dependence is exponential

$$\sigma = B \cdot e^{-\frac{E_c}{t}} + \sigma_0;$$
(11)

as we can see on *Figure 8b*. Then the matrix element of our response function can be written as

$$h^{ij} = C^j \cdot e^{-2\left(\dfrac{E^i - E_c{}^j}{B \cdot e^{-\frac{E_c{}^j}{t}} + \sigma_0}\right)^2} ; \qquad (12)$$

where C^j is a normalization constant.

$$C^j = \dfrac{1}{\sum_i e^{-2\left(\dfrac{E^i - E_c{}^j}{B \cdot e^{-\frac{E_c{}^j}{t}} + \sigma_0}\right)^2}} ; \qquad (13)$$

Each row of the matrix was normalized to unity in order to preserve the integral under cross section curves during deconvolution processing. Because deconvolution processing is very sensitive to the shape of the curve and position of its maximum, we decided to fit cross section curves with Gaussian functions. The Gaussian functions were processed by using the deconvolution method. The initial data were then multiplied by the acquired coefficient for each energy value.
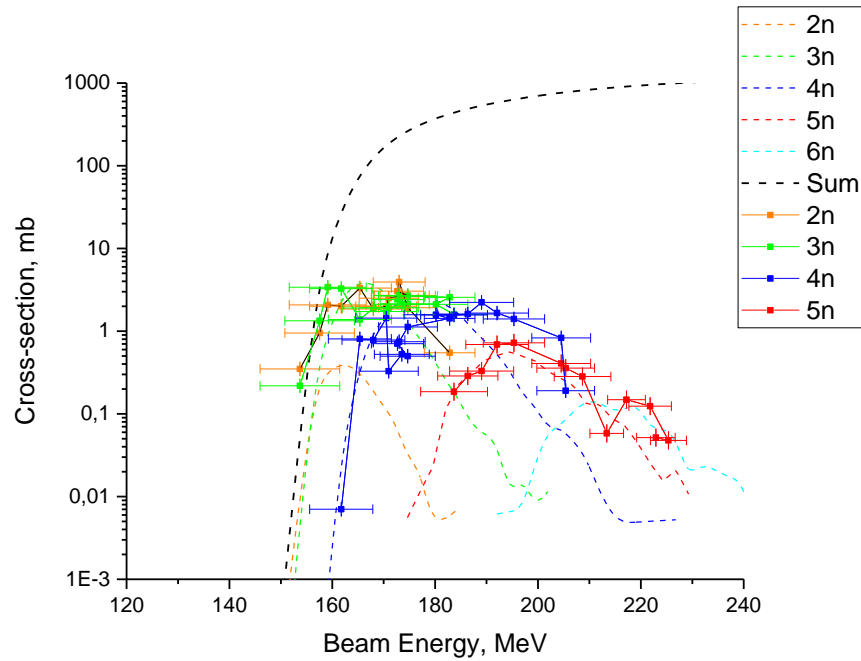

Figure 9. *Determined cross sections (symbols) of xn-evaporation channels (2n-orange, 3n-green, 4n-blue, 5n-red, 6n-purple, dash-line – NRV theoretical data, solid line – practically obtained data) of the reactions of synthesis ³⁶Ar + ¹⁴⁸Sm, measured by using the catcher foil method.*

RESULTS DISCUSSION

Experimental results for the measured reaction are shown in *Figure 9.* Experimental cross sections are drawn by using colored symbols (*2n*-orange, *3n*-green, *4n*-blue, *5n*-magenta and *6n*-purple). Individual points are linked by lines for better clarity. Cross sections calculated by using the channel-coupling model are drawn with dashed lines. The dashed black line represents the calculated summary cross section for fusion. All data were processed by applying half-life and alpha decay probability corrections. The half-life adjustment was considered by the working group for the reactions.

In this work the calculation of cross-sections was performed for the reaction $^{148}Sm(^{36}Ar,xn)^{184-x}Hg$, the remaining reactions such as $^{144}Sm(^{40}Ar,xn)^{184-x}Hg$, $^{144}Nd(^{40}Ca,xn)^{184-x}Hg$, $^{142}Nd(^{48}Ca,xn)^{190-x}Hg$, and $^{166}Er(^{40}Ar,xn)^{206-x}Rn$ were considered by the working team. When comparing the results it was found that the use of the deconvolution method has a significant influence on the shape of the cross-section curves in reactions with the largest amount of decreased beam energy (reactions with ^{36}Ar and ^{40}Ar beams) whilst this influence is minimal in the reaction with the lowest amount of decreased beam energy ($^{48}Ca + ^{142}Nd$).

$2n$ and $3n$ channels dominate in the reaction $^{40}Ar + ^{144}Sm$ with a similar maximal value of cross-section ($\sigma_{2n} = 13$ mb and $\sigma_{3n} = 12,4$ mb), while cross-sections of channels with a higher number of evaporated neutrons decreases gradually, because fission channels are still more important in higher excited states ($\sigma_{4n} = 5,4$ mb, $\sigma_{5n} = 1,5$ mb a $\sigma_{6n} = 0,03$ mb).

The Coulomb barrier for this system reaches a value of 39 MeV, which means that for energies lower than this value the reaction mechanism is dominated by sub-barrier fusion. This is the main cause for the considerably lower value of the $1n$ channel cross section, which we were not able to distinguish in measured spectra.

A similar behavior could be seen in the reaction $^{36}Ar + ^{148}Sm$ (*Figure 9*), which leads to the same isotopes ($\sigma_{2n} = 3,92$ mb, $\sigma_{3n} = 3,39$ mb, $\sigma_{4n} = 2,23$ mb a $\sigma_{5n} = 0,72$

mb). However, unlike the reaction $^{40}Ar + {}^{144}Sm$, which is a reaction of two spherical nuclei, here both nuclei are deformed.

In reactions of deformed nuclei, the height of the Coulomb barrier depends on the orientation of the participating nuclei [6]. Therefore, two values of the Coulomb barrier are given, which were calculated by the working team.

One for mutual polar orientation of nuclei, $V_P = 42$ MeV, and a second for equatorial orientation, $V_R = 49$ MeV. The threshold value of the excitation energy for total fusion in the reaction $^{40}Ar + {}^{144}Sm$ is approximately 27 MeV, while in the reaction $^{36}Ar + {}^{148}Sm$ it is around 35 MeV. This difference is a result of the different Q values of these reactions (-90,7 MeV for $^{40}Ar + {}^{144}Sm$ vs. -83,2 MeV for $^{36}Ar + {}^{148}Sm$). Different threshold values of these reactions cause a difference in locations of the $2n$ channel cross-section maximums, approximately 5 MeV, while the locations of maximal values of channels with higher numbers of evaporated nuclei are approximately the same.

Also, it was presented in the work of [7], where it turned out similar results with the overestimated value of the cross-section relative to theoretical data.

This difference is highlighted in *Figure 9*. The threshold value of the excitation energy causes suppression of lower energy portions of $2n$ and $3n$ channels in reaction.

By comparison of calculated and experimentally determined cross-sections it is apparent that all reactions leading to mercury isotopes have slightly higher values of cross section compared to calculations. The largest difference between data and calculations is seen in the *2n* channel of the reaction $^{36}Ar + {}^{148}Sm$. Cross section maximal values and their positions for all reactions are listed in *Table 5*.

Table 5. *Cross section maximal values in individual channels of fusion reactions and their position in the excitation energy scale.*

Reactions	Cross sections, σ[mb]				
	2n	3n	4n	5n	6n
$^{40}Ar + {}^{144}Sm \rightarrow {}^{184}Hg$	13	12,4	5,42	1,49	0,39
$^{36}Ar + {}^{148}Sm \rightarrow {}^{184}Hg$	3.92	3.39	2.23	0.72	-

CONCLUSION

Evaporation residue cross-sections in the reaction $^{36}Ar(^{148}Sm, xn)$ were measured by using the catcher foil method.

Experimental results for all measured reactions are shown in *Figure 9* as a function of excitation energy. Experimental cross sections are drawn by using colored symbols (*2n*-orange, *3n*-green, *4n*-blue, *5n*-red). Cross-sections calculated by using the NRV [8] data are drawn with dashed lines. All data were processed by applying half-life and alpha decay probability corrections.

Energies were measured by using a TDC, and energy losses were counted by using SRIM software. Cross-section errors are calculated as the root of the quadratic sum of statistical error, error linked with data processing, error of beam current measurement, and target measurement error.

REFERENCES

[1]   Y. Oganessian et al., Measurements of cross sections and decay properties of the isotopes of elements 112, 114, and 116 produced in the fusion reactions ^{233,238}U, ^{242}Pu, and ^{248}Cm + ^{48}Ca, Physical Review C, vol. 70, Issue 6 (2004)

[2]   A. M. Rodin et al., MASHA Separator on the Heavy Ion Beam for Determining Masses and Nuclear Physical Properties of Isotopes of Heavy and Superheavy Elements, Instruments and Experimental Techniques, Vol. 57, No. 4, pp. 386–393 (2014)

[3]   D. Vermeulen, H.G. Clerc, C.C. Sahm, K.H. Schmidt, J.G. Keller, G. Mtinzenberg, and W. Reisdorf, Cross Sections for Evaporation Residue Production near the N = 126 Shell Closure, Z. Phys. A - Atoms and Nuclei 318, 157-169 (1984)

[4]   J.F. Ziegler, M.D Ziegler, J.P Biersack, SRIM - The stopping and range of ions in matter, Nuclear Instruments and Methods in Physics Research Section B, Volume 268, Issue 11-12, p. 1818-1823 (2010)

[5]   M. Morhac, J. Kliman, V. Matousek, M. Veselsky, I. Turzo, Efficient one- and two-dimensional gold deconvolution and its application to y-ray spectra decomposition, Nuclear Instruments and Methods in Physics Research A 401, 385-408 (1997)

[6]   P. Möller, A.J. Sierk, T. Ichikawa, H. Sagawa, Atomic Data and Nucl. Data Tables, 109-110, 1-204 (2016)

[7]   M.Schädel et al, Cross sections measurement in fusion reactions ^{36}Ar(^{148}Sm, xn), GSI report, 2003.

[8]   A.V. Karpov et al., NRV web knowledge base on low-energy nuclear physics, Nuclear Instruments and Methods in Physics Research, Section A: Accelerators, Spectrometers, Detectors and Associated Equipment, Volume 859, 1 July 2017, Pages 112-124 (2017)